

# On the temporal tweezing of cavity solitons

Julia Rossi<sup>1</sup>, Sathyanarayanan Chandramouli<sup>2</sup>,  
Ricardo Carretero-González<sup>1</sup>, Panayotis G. Kevrekidis<sup>2</sup>

<sup>1</sup>Nonlinear Dynamical Systems Group\*, Computational Science Research Center<sup>†</sup>, and Department of Mathematics and Statistics, San Diego State University, San Diego, 92182-7720, California, USA.

<sup>2</sup>Department of Mathematics and Statistics, University of Massachusetts, Amherst, 01003-4515, Massachusetts, USA.

## Abstract

Motivated by the work of J.K. Jang et al., Nat. Commun. **6**, 7370 (2015), where the authors experimentally tweeze cavity solitons in a passive loop of optical fiber, we study the amenability to tweezing of cavity solitons as the properties of a localized tweezer are varied. The system is modeled by the Lugiato-Lefever equation, a variant of the complex Ginzburg-Landau equation. We produce an effective, localized, trapping tweezer potential by assuming a Gaussian phase-modulation of the holding beam. The potential for tweezing is then assessed as the total (temporal) displacement and speed of the tweezer are varied, and corresponding phase diagrams are presented. As the relative speed of the tweezer is increased we find two possible dynamical scenarios: successful tweezing and release of the cavity soliton. We also deploy a non-conservative variational approximation (NCVA) based on a Lagrangian description which reduces the original dissipative partial differential equation to a set of coupled ordinary differential equations for the cavity soliton parameters. We illustrate the ability of the NCVA to accurately predict the separatrix between successful and failed tweezing. This showcases the versatility of the NCVA to provide a low-dimensional description of the experimental realization of the temporal tweezing.

**Keywords:** Optical tweezers, cavity solitons, complex Ginzburg-Landau equation, Lugiato-Lefever equation, non-conservative Lagrangian formulation

---

\*URL: <http://nlds.sdsu.edu/>

<sup>†</sup>URL: <http://www.csrc.sdsu.edu/>

**Acknowledgments.** R.C.G. gratefully acknowledges support from the US National Science Foundation under Grants PHY-1603058 and PHY-2110038. P.G.K. gratefully acknowledges support from the US National Science Foundation under Grants DMS-2204702 and PHY-2110030.

## 1 Introduction

An optical tweezer, i.e., a single-beam gradient force trap, can capture, manipulate and move nanometer and micron-sized dielectric particles in space using a highly focused laser beam [1, 2]. Optical tweezers have been used in physics and biology to manipulate objects and measure forces [3]. The optical trapping and manipulation of the temporal position of light pulses is highly desirable as it may have direct implications for optical information processing. In this case, information is treated as a sequence of pulses that can be stored and reconfigured by trapping ultrashort pulses of light and dynamically moving them around in time. In particular, a temporal tweezer can exert similar control over ultrashort light pulses in time as reported in Ref. [4]. The optical trapping and manipulation of light pulses is useful in optical information processing [5–8] where the information is represented as a sequence of pulses. Temporal tweezing is an effective method to trap ultrashort pulses of light and move them around in *time* in order to store and reconfigure the information. Optical information processing is partly achieved in slow-light [9–12] and nonlinear cross-phase modulation effects [13–18], however neither approach allows for the independent control of light pulses within the sequence. It should be noted that solitary wave transfer in continuum and discrete (gain and loss) media has been previously illustrated, e.g., in Ref. [19], while the use of potentials (such as time-dependent optical [20, 21] or Bessel [22] lattices) has been used to drive solitary waves in atomic and optical systems. Such ideas of capture, release and overall control of the solitary waves have been popular in other areas too, including, e.g., in electrical lattice experiments [23]. Based on Ref. [4], we present a detailed analysis of temporal tweezing by means of direct numerical simulations as well as an analytical low-dimensional reduction of the wave’s dynamics based on a non-conservative variational approach (NCVA) [24].

We investigate temporal tweezing of cavity solitons in a passive loop of optical fiber pumped by a continuous-wave laser beam which is described by a modified Lugiato-Lefever (LL) partial differential equation (PDE) model which, in turn, is a special case of the celebrated complex Ginzburg-Landau equation [25, 26]. In the experiments described in Ref. [4], temporal cavity solitons (CSs) were created as picosecond pulses of light that recirculate in a loop of optical fiber and are exposed to temporal controls in the form of a gigahertz phase modulation. It has been shown, both theoretically and experimentally, that the CSs are attracted and trapped to phase maxima, suppressing all soliton interactions. These trapped CSs can then be manipulated in time, either forward or backward, which is known as temporal tweezing. We study the existence and dynamics of temporally tweezed CSs. The key phenomena reported herein are parametric regions separating the following tweezing scenarios: (i) successful temporal tweezing of the CS where the CS moves as prescribed by the tweezer and (ii) the failed tweezing regime where the effective potential moves too fast and leaves the CS behind.

We also apply the NCVA to reduce the LL dynamics of CSs to a set of ordinary differential equations (ODEs) on the CS parameter. We therefore, identify regions of temporal tweezing, and compare to the full numerical solutions of the original LL PDE. We find very good agreement between the two for the parametric regime considered, illustrating the ability of this effective reduction to provide an accurate characterization of the dynamics.

The manuscript is organized as follows. In Sec. 2 we introduce the temporal tweezing approach suggested in Ref. [4] and describe the LL model. We then add a Gaussian phase-modulation to the LL model and simulate the moving and manipulation of the CS. In Sec. 3 we provide a brief description of the NCVA approach and its formulation within the LL model. Then, the rest of the section is devoted to the application of the NCVA to capture the tweezing of a CS. In Sec. 4 we identify parameter regimes for the existence of trapped CSs and follow the tweezing dynamics from the ensuing manipulation of the phase-modulation of a continuous-wave holding beam. Finally, in Sec. 5 we summarize our key findings and provide possible avenues for future research.

## 2 The Full Model: Lugiato-Lefever Equation and Temporal Phase Modulation

In our analysis of temporal tweezing we begin with dissipative solitons in externally-driven nonlinear passive cavities, the so-called temporal CSs [27–32]. In a passive loop of optical fiber these light pulses can persist without losing shape because the dispersive temporal spreading is balanced by the material nonlinearity. Also, CSs persist without losing their intensity by drawing power from a continuous-wave (cw) “holding” laser beam driving the cavity. Multiple CSs may be simultaneously present in the optical loop and positioned independently temporally [33]. Here, we report on the trapping of CSs and the dynamical manipulation through selectively altering the phase profile of the holding beam.

### 2.1 Theory of Temporal Tweezing

Temporal tweezing requires a CS with an attractive time-domain drift towards the maxima of the intracavity phase profile. The attraction is due to the CSs shifting their instantaneous frequencies in response to a phase modulation. The gain and loss mechanisms inherent to this system may be captured by a variant of the celebrated complex Ginzburg-Landau (cGL) equation [25, 26]. In particular, following Refs. [4, 34, 35], we will model the system under consideration by the following Lugiato-Lefever (LL) equation:

$$z_R \frac{\partial E}{\partial z} = \left[ -\alpha - i\delta - iL \frac{\beta_2}{2} \frac{\partial^2}{\partial \tau^2} + i\gamma L |E|^2 \right] E + \sqrt{\theta} E_{\text{in}}, \quad (1)$$

where  $z$  is the slow time describing the intracavity field envelope  $E(z, \tau)$  and  $\tau$  is the fast time describing the temporal profile of the field envelope in a reference frame traveling at the group velocity of the holding beam in the cavity. The cavity roundtrip time is  $z_R$  and the field of the holding beam is  $E_{\text{in}}$  with power  $P_{\text{in}} = |E_{\text{in}}|^2$ . The

cavity losses are accounted by  $\alpha = \pi/\mathcal{F}$ , where  $\mathcal{F}$  is the cavity finesse. The phase detuning of the intracavity field to the closest cavity resonance of order  $l$  is given by  $\delta = 2\pi l - \phi_0$  where  $\phi_0$  is a linear phase-shift over one roundtrip with respect to the holding beam. Finally,  $L$  is the cavity length,  $\beta_2$  is the dispersion coefficient of the fiber,  $\gamma$  is the nonlinear coefficient of the fiber, and  $\theta$  is the input coupler power transmission coefficient.

In what follows, for ease of exposition, we will work in adimensional units. For that purpose, the LL Eq. (1) may be adimensionalized by introducing a dimensionless slow time  $z' = \alpha z/z_R$  and a dimensionless fast time  $\tau' = \tau\sqrt{2\alpha/(L|\beta_2|)}$ . We also use a dimensionless complex field amplitude  $v(z', \tau') = E(z, \tau)\sqrt{\gamma L/\alpha}$  and a dimensionless holding beam  $v_{\text{in}} = E_{\text{in}}\sqrt{\gamma L\theta/\alpha^3}$ . For convenience, we drop the primes in the notation of  $z'$  and  $\tau'$ , such that Eq. (1) becomes the dimensionless mean-field LL equation

$$\frac{\partial v}{\partial z} = -(1 + i\Delta)v + i|v|^2v + i\frac{\partial^2 v}{\partial \tau^2} + v_{\text{in}}, \quad (2)$$

where  $\Delta = \delta/\alpha$  is the effective dimensionless detuning and we have chosen  $\text{sgn}(\beta_2) = -1$ .

Homogeneous and steady ( $\tau$ - and  $z$ -independent) states,  $v(z, \tau) = v_s$ , of Eq. (2), where the CSs will be supported, satisfy

$$|v_s|^2 v_s = -iv_s + \Delta v_s + iv_{\text{in}}. \quad (3)$$

Defining the intracavity background field intensity  $I_s \equiv |v_s|^2$ , one can write the steady state solution in implicit form

$$v_s = \frac{v_{\text{in}}}{1 + i(\Delta - I_s)},$$

which displays the dependence on the detuning  $\Delta$  and holding beam power  $v_{\text{in}}$ . This implicit relationship may be cast in the form of a well-known cubic equation for dispersive optical bistability [6, 34, 36, 37]

$$I_s^3 - 2\Delta I_s^2 + (1 + \Delta^2)I_s = I_0, \quad (4)$$

where  $I_0 \equiv |v_{\text{in}}|^2$  is the holding beam intensity. For small detuning,  $\Delta < \sqrt{3}$ , Eq. (4) has only one solution for the the steady state  $I_s$  given a specific holding beam power  $v_{\text{in}}$ . For large detuning,  $\Delta > \sqrt{3}$ , there are three solutions for  $I_s$  given a specific holding beam power  $v_{\text{in}}$ . The homogeneous solution is bistable since two solutions are stable while the other solution is unstable.

We follow the approach of Refs. [4, 38] to study the effect of phase-modulation of the holding field. The phase-modulation is imprinted into a constant holding beam which creates an effective potential necessary to attract, trap, and manipulate a CS. We assume a phase-modulation temporal profile  $\phi(\tau)$  and rewrite the holding beam

using

$$v_{\text{in}}(\tau) = u_{\text{in}} \exp[i\phi(\tau)], \quad (5)$$

where  $u_{\text{in}}$  is a constant scalar (whose square corresponds to the intensity of the holding beam). Substituting Eq. (5) into Eq. (2) with the ansatz  $v(z, \tau) = u(z, \tau) \exp[i\phi(\tau)]$  yields

$$iu_z + |u|^2 u + u_{\tau\tau} - (\Delta + (\phi')^2)u + 2iu_{\tau}\phi' = -i(1 + \phi'')u + iu_{\text{in}}, \quad (6)$$

where primes denote derivatives with respect to  $\tau$ . The cw intracavity field on which the CSs are supported has the same phase modulation as that imposed on the external holding beam in this non-dimensional form. In this form, the phase modulation of the holding beam introduces the following terms affecting the dynamics of the field envelope: (i)  $(\phi')^2$  acts like an effective potential caused by the phase modulation, (ii) the term  $2iu_{\tau}\phi'$  describes the effect of drift through the gradient term  $u_{\tau}$  where  $2\phi'$  represents a drift “speed” [39], and (iii) the  $\phi''$  term induces an additional loss in the system caused by the phase modulation.

Steady state solutions of the LL Eq. (6) are subject to an additional constraint stemming from the balance condition  $dP/dz = 0$ , where

$$P = \int_{-\infty}^{\infty} |u|^2 d\tau,$$

is the total power (mathematically, the squared  $L^2$  norm) of the cavity solitons. The evolution of  $P$  can be found by multiplying Eq. (6) by  $u^*$ , as well as the complex conjugate of Eq. (6) by  $u$ , and then adding and integrating the resulting equations [40]. For the LL Eq. (6), it is straightforward to find the following constraint condition for a steady state solution:

$$\int_{-\infty}^{\infty} \left( -|u|^2 - \phi''|u|^2 - \phi'(u_{\tau}u^* + u_{\tau}^*u) + \text{Re}(u)u_{\text{in}} \right) d\tau = 0, \quad (7)$$

which can be rewritten as

$$\int_{-\infty}^{\infty} \left( -|u|^2 + \text{Re}(u)u_{\text{in}} \right) d\tau = 0, \quad (8)$$

which demonstrates the same power balance constraint, as expected, for (non)-tweezed cavity solitons. This power-balance constraint will need to be enforced in the system, and, in turn, will fix the homogeneous background pedestal  $v_s$ , upon choosing the detuning  $\Delta$  and holding beam  $u_{\text{in}}$  parameters.

## 2.2 Temporal tweezing of Cavity Solitons

Our analysis involves temporal cavity solitons described by LL Eq. (6) stored in a passive loop of optical fiber pumped by a cw laser beam. The tweezed CS is trapped into

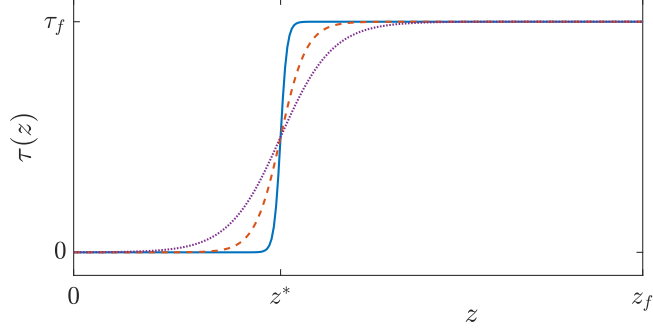


**Fig. 1** “Trajectory” of the temporal tweezing. The tweezer starts at  $\tau = 0$  and ends at  $\tau = \tau_f$ . The degree of adiabaticity is controlled with the parameter  $\beta$  in Eq. (11). The solid (blue) line represents a fast transition (relatively large  $\beta$ ) which will be less likely to tweeze the CS. With increasing degrees of adiabaticity (i.e., smaller values of  $\beta$ ), see dashed and dotted curves, it will be more likely for the tweezing to be successful.

a specific time slot through phase-modulation of the holding beam, and moved around in time by manipulating the phase profile. Experimentally, a modulator imprints a time-varying electric signal  $\phi(\tau)$  into the phase of the cw holding laser driving the cavity. For the purpose of the LL Eq. (6), we used a “natural” localized phase modulation with a Gaussian profile of the form

$$\phi(\tau) = h_\phi \exp\left(-\frac{(\tau - \tau_0)^2}{2\sigma_\phi^2}\right), \quad (9)$$

where  $h_\phi$ ,  $\sigma_\phi$ , and  $\tau_0$  describe, respectively, the height, width, and center position of the phase profile.

In what follows, we will first consider the stationary solutions of the LL model in the form  $u(z, \tau) = u_0(\tau)$  which are governed by the following ODE:

$$u_0'' + (|u_0|^2 - \Delta - (\phi')^2) u_0 + 2i\phi' u_0' = -i(1 + \phi'') u_0 + iu_{\text{in}}. \quad (10)$$

In practice, in what follows, the homogeneous background pedestal  $v_s$  is determined by solving algebraic equation Eq. (3) having made a choice for  $\Delta$  and  $u_{\text{in}}$ . This in turn fixes the boundary state ( $v_s$ ) for stationary CS states. Once stationary soliton solutions of the ODE Eq. (10) are identified (consistent with this boundary state) at  $\tau_0 = 0$ , their “temporal tweezeability” (i.e., amenability to transfer via tweezers) is considered by measuring the amount of soliton intensity that remains inside and outside of the effective potential  $(\phi')^2$  as the center location of the tweezer is (subsequently) manipulated.

To simulate moving and manipulating the cavity soliton through the phase profile we consider the following “motion” in the evolution variable  $z$ :

$$\tau_0(z) = \frac{\tau_f}{2} \left( \frac{\tanh[\beta(z - z^*)]}{\tanh(\beta z^*)} + 1 \right), \quad (11)$$

where  $\tau_f$  is the final fast time  $\tau$  at which the phase profile stops,  $z^*$  is the slow time for the phase profile to reach  $\tau_f/2$ , and  $\beta$  is the adiabaticity parameter which describes how fast the effective potential moves the temporal profile centered at  $\tau_0$ . Figure 1 depicts the trajectory of the temporal tweezer.

Having given the PDE setup of our considerations, we now turn to its effective low-dimensional description via the non-conservative variational approximation.

### 3 Non-conservative Variational Approximation

#### 3.1 Preliminaries

Let us now consider a semi-analytical method to dynamically reduce the LL equation to an effective “particle” picture described by a set of coupled ODEs on the CS parameters (height, position, width, phase, velocity, and chirp). We use the so-called non-conservative variational approximation (NCVA) for PDEs as described in Ref. [24]. This is inspired by the Lagrangian (and Hamiltonian) formulation of non-conservative mechanical systems originating in the work of Refs. [42, 43]; see also Ref. [44]. For completeness, let us briefly describe the NCVA approach (for more details please consult Ref. [24]). To employ the NCVA, we consider two sets of coordinates  $u_1$  and  $u_2$ . As proposed by Galley and collaborators [42, 43], the coordinates are fixed at an initial time ( $z_i$ ), but are not fixed at the final time ( $z_f$ ). After applying variational calculus for a non-conservative system, both paths are set equal,  $u_1 = u_2$ , and identified with the physical path  $u$ , the so-called physical limit (PL). The action functional for  $u_1$  and  $u_2$  is defined as the total line integral of the difference of the Lagrangians between the paths plus the line integral of the functional  $\mathcal{R}$  which describes the generalized non-conservative forces and depends on both paths:

$$S = \int_{z_i}^{z_f} (\mathcal{L}(u_1, u_{1,z}, u_{1,\tau}, \dots, z) - \mathcal{L}(u_2, u_{2,z}, u_{2,\tau}, \dots, z) + \mathcal{R}) dz,$$

where the  $z$  and  $\tau$  subscripts denote partial derivatives with respect to these variables. The above action defines a new total Lagrangian:

$$\mathcal{L}_T \equiv \mathcal{L}_1 - \mathcal{L}_2 + \mathcal{R},$$

where the first two terms represent the conservative Lagrangian densities with  $\mathcal{L}_i \equiv \mathcal{L}(u_i, u_{i,z}, u_{i,\tau}, \dots, z)$ , for  $i = 1, 2$ , and  $\mathcal{R}$  contains all non-conservative terms. For convenience,  $u_+ = (u_1 + u_2)/2$  and  $u_- = u_1 - u_2$  are defined in such a way that at the physical limit  $u_+ \rightarrow u$  and  $u_- \rightarrow 0$ . The equations of motion then yield

$$\frac{\partial}{\partial z} \left( \frac{\delta \mathcal{L}}{\delta u_z^*} \right) = \frac{\delta \mathcal{L}}{\delta u^*} + \left[ \frac{\delta \mathcal{R}}{\delta u_-^*} \right]_{\text{PL}}, \quad (12)$$

where  $\delta$  denotes the Fréchet derivatives. Through this method, we recover the Euler-Lagrange equation for the conservative terms and all non-conservative terms are

folded into  $[\delta\mathcal{R}/\delta u_-^*]_{\text{PL}}$ . It is crucial to construct the term  $\mathcal{R}$  such that its derivative with respect to the difference variable  $u_-$  at the physical limit gives back the non-conservative or generalized forces. This part concludes the field-theoretic formulation of the non-conservative problem and so far no approximation has been utilized. In what follows, we will proceed to solve the above Euler-Lagrange equations using an appropriate ansatz to *approximately* describe the CS solutions in this non-conservative Lagrangian formulation. Towards this end, we wish to study the dynamics of the solution restricted on what we will refer to as a “solitonic manifold”, i.e.  $u \equiv \bar{u}(\tau, \vec{p}(z))$ , for which the modified Euler-Lagrange equations for the effective Lagrangian  $\bar{L} = \int_{-\infty}^{\infty} \bar{\mathcal{L}} d\tau$  yield

$$\frac{d}{dz} \left( \frac{\partial \bar{L}}{\partial \dot{\vec{p}}} \right) - \frac{\partial \bar{L}}{\partial \vec{p}} - I_{\vec{p}} = 0, \quad (13)$$

where the integrals  $I_{\vec{p}}$  are given by  $I_{\vec{p}} \equiv \int_{-\infty}^{\infty} [\partial \bar{\mathcal{R}} / \partial \vec{p}_-]_{\text{PL}} d\tau$  and the overline indicates that the equations of motion have been evaluated on the approximate variational ansatz.

### 3.2 NCVA of Tweezed Cavity Solitons

We now describe the use of an approximate variational ansatz to describe the statics and dynamics of CSs subjected to the tweezing generated by the external terms induced by the phase variations of the holding beam. In particular, we apply the NCVA approach to Eq. (6) to analytically identify the tweezability regions in parameter space by following the solutions to the corresponding reduced system of ODEs given by the Euler-Lagrange Eqs. (13), restricting the original infinite-dimensional dynamics to the low-dimensional dynamics of the solitonic manifold (governing the evolution of the coherent structures characteristic features). The CS solution for the LL model sits on a pedestal (background). Therefore, we construct  $u = v_s + \bar{u}$  where  $\bar{u}$  is the NCVA ansatz and  $v_s$  is the homogeneous steady-state pedestal solution described in Eq (3). Applying the new construction of  $u$  into Eq. (6) produces the following modified LL equation for  $\bar{u}$ :

$$\begin{aligned} i\bar{u}_z + |\bar{u}|^2 \bar{u} + \bar{u}_{\tau\tau} - (\Delta + (\phi')^2 - 2|v_s|^2) \bar{u} + 2i\bar{u}_{\tau}\phi' + i\phi''\bar{u} = \\ -i\bar{u} + (-2|\bar{u}|^2 + (\phi')^2 - i\phi'')v_s - (v_s)^2 \bar{u}^* - (\bar{u})^2 v_s^* \end{aligned} \quad (14)$$

where we have used Eq. (3) to slightly simplify the resulting equation. The conservative part of the LL equation, namely the left-hand side of Eq. (14), originates from the following Lagrangian density:

$$\bar{\mathcal{L}}_{\text{cons}} = \frac{i}{2} (\bar{u}\bar{u}_z^* - \bar{u}^*\bar{u}_z) + |\bar{u}_{\tau}|^2 - \frac{1}{2}|\bar{u}|^4 + (\Delta + (\phi')^2 - 2|v_s|^2) |\bar{u}|^2 - i\phi' (\bar{u}^*\bar{u}_{\tau} - \bar{u}\bar{u}_{\tau}^*).$$

On the other hand, to construct the Lagrangian density leading to the non-conservative

part of the LL equation, namely the right-hand side of Eq. (14), we must find  $\mathcal{R}$  such that

$$\left[ \frac{\partial \bar{\mathcal{R}}}{\partial \bar{u}_-^*} \right]_{\text{PL}} = -i\bar{u} + (-2|\bar{u}|^2 + (\phi')^2 - i\phi'')v_s - (v_s)^2\bar{u}^* - (\bar{u})^2v_s^* \quad (15)$$

and thus, an appropriate choice for the non-conservative terms yields

$$\bar{\mathcal{R}} = \left[ -i\bar{u}_+ + (-2|\bar{u}_+|^2 + (\phi')^2 - i\phi'')v_s - (v_s)^2\bar{u}_+^* - (\bar{u}_+)^2v_s^* \right] \bar{u}_-^* + c.c., \quad (16)$$

where *c.c.* denotes the complex conjugate of the preceding term [it is necessary to choose this term to be the integration constant that arises upon integrating Eq. (15) to ensure the underlying NCVA parameters are real-valued]. Thus, the relevant Lagrangian density containing conservative and non-conservative terms can be written as

$$\bar{\mathcal{L}} = \bar{\mathcal{L}}_{\text{cons}}(\bar{u}_1) - \bar{\mathcal{L}}_{\text{cons}}(\bar{u}_2) + \bar{\mathcal{R}}, \quad (17)$$

where  $\bar{u}_1 = (2\bar{u}_+ + \bar{u}_-)/2$  and  $\bar{u}_2 = (2\bar{u}_+ - \bar{u}_-)/2$  and the expression for  $\bar{\mathcal{R}}$  is given in Eq. (16). In order to obtain analytical insights into the dynamics of the model, our aim is to use an ansatz approximation of the intracavity field envelope soliton reducing its original Lagrangian to a Lagrangian over effective (yet slowly varying) properties. Therefore, to approximate the CSs, we chose a six-parameter,  $\vec{p} = (a, \xi, \sigma, b, c, d)$ , Gaussian ansatz of the form:

$$\bar{u}_j = a_j \exp \left[ -\frac{(\tau - \xi_j)^2}{2\sigma_j^2} \right] \exp [i(d_j(\tau - \xi_j)^2 + c_j(\tau - \xi_j) + b_j)] \quad (18)$$

for  $j = 1$  and  $2$ , where the CS variational parameters correspond to height  $a$ , center position  $\xi$ , width  $\sigma$ , phase  $b$ , velocity  $c$ , and chirp  $d$ . It is relevant to mention that, as shown in Ref. [45], it is necessary to add chirp into the ansatz since the original model is out of equilibrium. As a consequence, for non-trivial solutions, there must exist internal (fluid) flows from regions of effective gain to regions of effective loss. These balancing flows correspond, in turn, to spatial variations of the phase that must be accounted by the chirp term.<sup>1</sup>

Following the NCVA methodology for ansatz (18), we obtain a system of ODEs [derived from Eq. (13)] for the variational parameters  $\vec{p}$ , which are listed in Appendix A. The resulting NCVA ODEs are cumbersome in their explicit form in that they include the terms  $I_a$ ,  $I_b$ ,  $I_c$ ,  $I_d$ ,  $I_\sigma$ , and  $I_\xi$  which involve integrals. In order to simplify these integrals, we recast the ansatz of Eq. (18) using its amplitude and phase as follows

$$\bar{u}(\tau, \vec{p}(z)) = \mathcal{A}(a, \sigma, \xi) \exp[i\Phi(b, c, d, \xi)],$$

---

<sup>1</sup>The connection between phase variations and (fluid) flows can be elucidated within setups corresponding to the cGL equation with real coefficients; namely NLS-type equations. Within NLS-type models, the Madelung transformation (that separates the wavefunction in density and phase terms) allows recasting the original NLS PDE into a modified (by the so-called quantum pressure term) non-viscous Eulerian fluid where, importantly, the gradient of the phase precisely corresponds to the fluid velocity [46].

where  $\mathcal{A}(a, \sigma, \xi) \equiv a \exp(-(\tau - \xi)^2/(2\sigma^2))$  and  $\Phi(b, c, d, \xi) \equiv b + c(\tau - \xi) + d(\tau - \xi)^2$  for variational parameters  $\vec{p} = (a, b, c, d, \sigma, \xi)$ . These integrals for all the variational parameters  $p_i$  are of the form, by leveraging the equivalence of the NCVA with the Kantorovitch method [24]:

$$I_{p_i} = 2 \operatorname{Re} \int_{-\infty}^{\infty} \left[ -i\bar{u} + (-2|\bar{u}|^2 + (\phi')^2 - i\phi'')v_s - (v_s)^2\bar{u}^* - (\bar{u})^2v_s^* \right] \frac{\partial \bar{u}^*}{\partial p_i} d\tau.$$

Therefore, using the notation  $\mathcal{A}_{p_i} = \partial \mathcal{A} / \partial p_i$ ,  $\Phi_{p_i} = \partial \Phi / \partial p_i$ ,  $v_I = \operatorname{Im}(v_s)$ ,  $v_R = \operatorname{Re}(v_s)$ ,  $\kappa = -4\mathcal{A}^2 + 2(\phi')^2$  and  $\mathcal{X}^{(i)} = \frac{\partial \bar{u}^*}{\partial p_i}$ , together with  $\operatorname{Re}(\mathcal{X}^{(i)}) = \mathcal{X}_R^{(i)}$  and  $\operatorname{Im}(\mathcal{X}^{(i)}) = \mathcal{X}_I^{(i)}$ , we can write a general form for  $I_{p_i}$  as follows:

$$I_{p_i} = \int_{-\infty}^{\infty} \left( -2\mathcal{A}^2\Phi_{p_i} + \Gamma_1^{(i)} \cos(\Phi) + \Gamma_2^{(i)} \sin(\Phi) + \Gamma_3^{(i)} \cos(2\Phi) + \Gamma_4^{(i)} \sin(2\Phi) \right) d\tau,$$

where  $\Gamma_j^{(i)}$ ,  $j = 1, 2, 3, 4$  are defined through the following expressions

$$\begin{aligned} \Gamma_1^{(i)} = & \kappa v_R \mathcal{A}_{p_i} + \kappa v_I \mathcal{A} \Phi_{p_i} - 2\phi'' v_R \mathcal{A} \Phi_{p_i} + 2\phi'' v_I \mathcal{A}_{p_i} \\ & + 2(v_I^2 - v_R^2) \mathcal{A} \mathcal{X}_R^{(i)} + 4v_I v_R \mathcal{A} \mathcal{X}_I^{(i)} \end{aligned} \quad (19)$$

$$\begin{aligned} \Gamma_2^{(i)} = & -\kappa v_R \mathcal{A} \Phi_{p_i} + \kappa v_I \mathcal{A}_{p_i} - 2\phi'' v_R \mathcal{A}_{p_i} - 2\phi'' v_I \mathcal{A} \Phi_{p_i} \\ & + 2(v_I^2 - v_R^2) \mathcal{A} \mathcal{X}_I^{(i)} - 4v_I v_R \mathcal{A} \mathcal{X}_R^{(i)} \end{aligned} \quad (20)$$

$$\Gamma_3^{(i)} = -2\mathcal{A}^2(v_R \mathcal{X}_R^{(i)} + v_I \mathcal{X}_I^{(i)}) \quad (21)$$

$$\Gamma_4^{(i)} = 2\mathcal{A}^2(v_R \mathcal{X}_I^{(i)} - v_I \mathcal{X}_R^{(i)}) \quad (22)$$

Succinctly, the expressions for  $\mathcal{X}_R^{(i)}$  and  $\mathcal{X}_I^{(i)}$  can be written as the following system:

$$\begin{bmatrix} \mathcal{X}_R^{(i)} \\ \mathcal{X}_I^{(i)} \end{bmatrix} = \begin{bmatrix} \cos(-\Phi) & -\sin(-\Phi) \\ \sin(-\Phi) & \cos(-\Phi) \end{bmatrix} \begin{bmatrix} \mathcal{A}_{p_i} \\ -\mathcal{A} \Phi_{p_i} \end{bmatrix}. \quad (23)$$

Although  $I_{p_i}$  may appear cumbersome, the integrals are reduced by the presence (or not) of the derivatives  $\mathcal{A}_{p_i}$  and  $\Phi_{p_i}$ , e.g.,  $\mathcal{A}_b = \mathcal{A}_c = \mathcal{A}_d = 0$  and  $\Phi_a = \Phi_\sigma = 0$ . The only derivatives that are of importance are:

$$\begin{aligned} \mathcal{A}_a &= \frac{\mathcal{A}}{a}, \quad \mathcal{A}_\sigma = \frac{(\tau - \xi)^2}{\sigma^3} \mathcal{A}, \quad \mathcal{A}_\xi = \frac{\tau - \xi}{\sigma^2} \mathcal{A}, \\ \Phi_b &= 1, \quad \Phi_c = \tau - \xi, \quad \Phi_\xi = -c - 2d(\tau - \xi), \quad \Phi_d = (\tau - \xi)^2. \end{aligned}$$

All the relevant integrals are approximated numerically to spectral accuracy with the trapezoidal rule (see Ref. [50]).

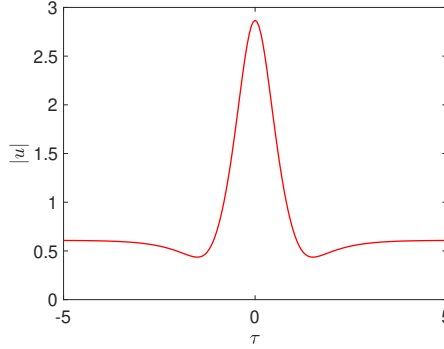


**Fig. 2** A LL CS profile (where the profile of  $|u|$  is shown) recovered for parameters  $\Delta = 3.5$  and  $u_{\text{in}} = 2$  in the absence of the phase modulation  $\phi(\tau) \equiv 0$ .

Let us now use the NCVA equations of motion both to seek to capture the stationary CS states, as well as to describe the dynamics of CSs subject to the tweezing in Eq. (11) in order to assess its tweezability as a function of  $\tau_f$  (how far we want to tweeze) and  $\beta$  (how adiabatic is the tweezing).

## 4 Results

### 4.1 Determination of (non-)tweezed stable CS states

As a precursor to performing the temporal tweezing study, we first identify an appropriate regime in the parameters (i)  $u_{\text{in}}$  and  $\Delta$  and subsequently the phase modulation parameters (ii)  $h_\phi$  and  $\sigma_\phi$  [in Eq. (9)]. By the term “appropriate” here, we mean a regime where the CS state is spectrally stable both in the absence of the tweezer (in the bulk LL setting), as well as in the presence of the tweezer, so that it be amenable to dynamical tweezing. Crucially, this determination leads to suitable stable CS states which can be successfully temporally tweezed for some non-trivial regime in the adiabaticity ( $\beta$ ) and final fast time ( $\tau_f$ ) parameters [defined by the temporal tweezing of Eq. (11)].

Two remarks are in order:

- (a) As alluded to earlier, the computation of fixed points to the ODE of Eq. (10) is initiated by first fixing the homogeneous background pedestal  $v_s$  [obtained as a solution to Eq. (3)] with a choice of the parameters  $\Delta$  and  $u_{\text{in}}$ . Notably, this background state  $v_s$  stays fixed in the presence of the localized phase modulation  $\phi(\tau)$  as well [cf. Eq. (8)]. Thereafter, we employ the Newton-conjugate gradient iterative scheme [51] to recover the CS profiles in  $\bar{u}_0(\tau) = u_0(\tau) - v_s$ . To study the stability of the CS, we linearize Eq. (14) around these stationary states by inserting the ansatz  $\bar{u} = \bar{u}_0 + \epsilon(f(\tau)\exp(i\omega z) + g^*(\tau)\exp(-i\omega^*z))$ , for  $\epsilon \ll 1$ , which yields the following linear stability (eigenfrequency) problem (at order  $\epsilon$ ) upon collecting

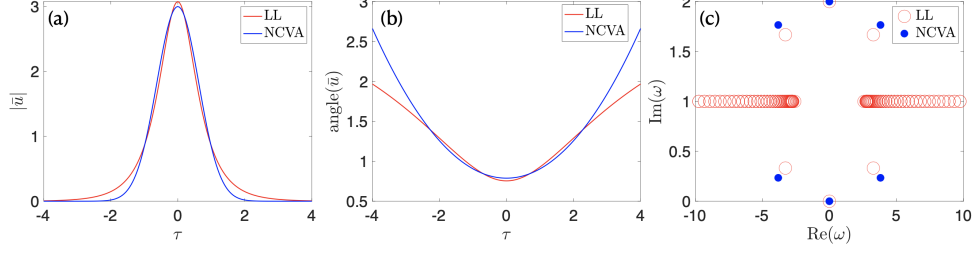


**Fig. 3** A comparison of the CS profile at the NCVA and LL PDE levels for parameters  $\Delta = 3.5$  and  $u_{\text{in}} = 2$  in the absence of the phase modulation  $\phi \equiv 0$ . Comparison of the (a) amplitude and (b) phase of the CS for the LL model (red) and its NCVA counterpart (blue). (c) Stability spectra of the CS for the LL model (red circles) together with its NCVA counterpart (blue dots).

the coefficients of  $\exp(i\omega z)$  and  $\exp(-i\omega^* z)$

$$\begin{bmatrix} A + \partial_{\tau\tau} & B \\ -B^* & -A^* - \partial_{\tau\tau} \end{bmatrix} \begin{bmatrix} f \\ g \end{bmatrix} = \omega \begin{bmatrix} f \\ g \end{bmatrix}, \quad (24)$$

where  $A \equiv 2|\bar{u}_0|^2 - (\Delta + (\phi')^2 - 2|v_s|^2) + i\phi'' + i + 2v_s\bar{u}_0^* + 2v_s^*\bar{u}_0$  and  $B \equiv \bar{u}_0^2 + 2v_s\bar{u}_0 + v_s^2$ , for the eigenfrequency  $\omega$ .

- (b) We complement our studies at the level of the LL Eq. (6) with analogous investigations at the level of the NCVA ODE system (see Appendix A). We compute fixed points to this ODE system  $\dot{\vec{p}} = \vec{F}(\vec{p})$  by solving a six-dimensional algebraic system  $F(\vec{p}) = 0$  using a Newton-based black box-solver `nsoli.m` [52]. The NCVA eigenfrequencies  $\omega_0$  of the corresponding  $6 \times 6$  Jacobian  $\partial \vec{F} / \partial \vec{p}$  can also be used as an appropriate diagnostic to characterize linear stability of stationary states, and thus predict successful temporal tweezing. Importantly, also, the resulting values of  $\omega_0$  are directly compared with the spectral stability findings at the level of the LL PDE, as yet another layer of comparison regarding the accuracy of the NCVA approach.

After an extensive line search in  $\Delta$  (for fixed  $u_{\text{in}} = 2$ ), we find that for  $\Delta \gg \sqrt{3}$ , stable CS are recovered for  $\phi(\tau) \equiv 0$ . Furthermore, their stability is reflected at the level of the NCVA ODE system as well. The profile ( $|u|$ ) of such a LL CS is depicted in Fig. 2. Next, we showcase the ability of the NCVA approach to capture the statics and stability of the original CSs in the LL equation. In particular, panels (a) and (b) of Fig. 3 depict a typical comparison between shape and phase profiles of the NCVA and LL CS. The figure evidenced that the NCVA is able to give a good approximation of the exact CSs. Furthermore, panel (c) depicts the associated linear stability spectra  $\omega$  for both the NCVA and the LL CS. Note that for the choice of parameters, the spectra lie entirely above the lower half plane, i.e., have  $\text{Im}(\omega) \geq 0$ , confirming stability. Additionally, and reassuringly, the stability eigenvalues of the NCVA ODE system (blue dots) are also seen to demonstrate reasonable quantitative agreement with the discrete spectra of the original LL CS.

Next, we consider the case of adiabatically turning on the phase modulation, in the presence of a bulk ( $\phi \equiv 0$ ) LL CS having fixed  $\Delta = 3.5$  and  $u_{\text{in}} = 2$ . Figure 4 depicts a

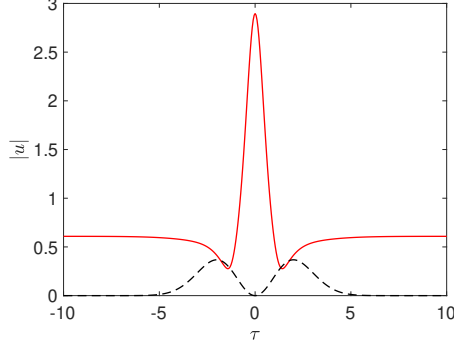


**Fig. 4** A stationary LL CS profile (in terms of  $|u|$ ; see red curve) in the presence of the effective potential (see black dashed curve) ensuing from the phase modulation spatial profile. This case corresponds to the parameters  $\Delta = 3.5$ ,  $u_{\text{in}} = 2$ ,  $h_\phi = 2$ , and  $\sigma_\phi = 2$  in the presence of the phase modulation  $\phi(\tau)$  described in Eq. (9).

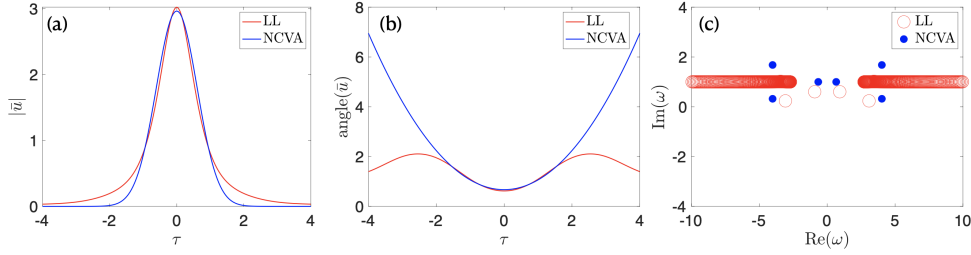


**Fig. 5** A comparison of the stationary CS profile (with the pedestal factored out) in the presence of the phase modulation, at the NCVA and LL PDE levels for parameters  $\Delta = 3.5$ ,  $u_{\text{in}} = 2$ ,  $h_\phi = \sigma_\phi = 2$ : Comparisons (a) of the amplitude variations of the LL CS (in red), and the NCVA counterpart in blue, (b) the phase variations of the LL CS (in red) and the NCVA counterpart in blue and (c) the LL stability spectra plotted against the NCVA stability eigenvalues.

typical tweezed CS and the corresponding effective trapping potential originating from the phase modulation. We find that for shallow effective potential, i.e.  $\max_\tau (\phi')^2 \ll 1$ , both the NCVA and the LL models support CSs that are stable as showcased in Fig. 5. This stability of the confined CS (within the phase modulation) is crucial towards a potential successful tweezing of such localized states. As for the untrapped case, the NCVA predicts stability for this trapped CSs. For the remainder of the paper, we fix  $h_\phi = 2$  and  $\sigma_\phi = 2$ . The choice of these phase modulation parameters will allow us to demonstrate successful not only static, but also dynamic tweezability, as we will now show.

## 4.2 Temporal tweezing

We now explore the existence and dynamical properties for a tweezed cavity soliton in the effective potential described by  $V_{\text{eff}} = (\phi')^2$  (also referred to as the “tweezer”). Before embarking on the dynamical tweezability of CSs, we must know what are the

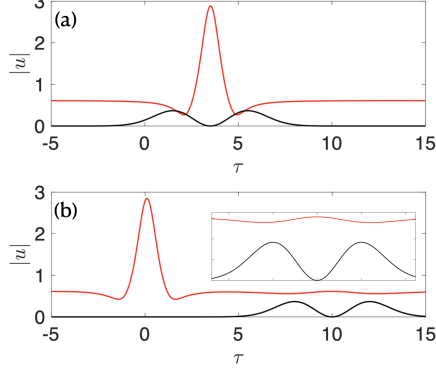


**Fig. 6** Temporal profiles of the intracavity field envelope  $|u|^2$  (red line) for the two fundamental CS states of the system. In this example, the effective potential,  $V_{\text{eff}} = (\phi')^2$  (solid black line) is varying in the evolution variable in the two panels with parameters  $\sigma_\phi = 2$  and  $h_\phi = 2$ . The top panel is an example of a trapped CS by the time-dependent effective potential (i.e., a successfully tweezed CS). The bottom panel is an example of a failed tweezing attempt. Note that in this case, a small amplitude localized state is observed within the tweezing potential, which can be viewed as a modulation of the homogeneous background pedestal.

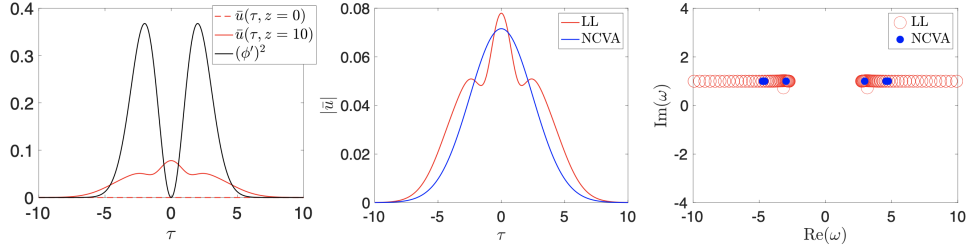


**Fig. 7** (a) A localized state arises within the effective potential (shown in black solid line) as a steady state past  $z = 10$ , (red solid line) when initialized with the homogeneous pedestal (red dashed line). Here the field variable  $|\bar{u}| = |u - v_s|$  is shown to describe the waveforms. (b) The NCVA successfully captures this localized state: the panel shows the amplitude profile of the localized modulation at the level of the LL (red solid) and its NCVA analog (blue solid). (c) The LL and NCVA stability spectra (eigenvalues) confirm the stability of this localized feature within the confining potential. The absence of point spectrum modes here indicates that this is the analog of the homogeneous state in the presence of the phase-modulation-induced confinement.

different possible scenarios. In particular, for a tweezer there are two fundamental states corresponding to the following qualitatively different scenarios: (a) a CS inside the tweezer (also of relevance to the case of successful dynamical tweezing) and (b) a bulk CS outside of the tweezer, arising also in the setting of non-tweezed (or unsuccessfully tweezed) CS. These two scenarios are depicted in Fig. 6 for  $\sigma_\phi = 2$  and  $h_\phi = 2$  (which corresponds to a shallow tweezer). Interestingly, in the absence of the CS within the tweezer, a very small amplitude, localized, modulation of the background emerges within the effective potential created by the phase modulation [see Fig. 7(a)]. Notably,

this small amplitude modulation of the background can also be captured by the Gaussian NCVA ansatz, as shown in Fig. 7(b), and is a stable waveform, as illustrated in Fig. 7(c).

If we now consider a dynamically varying tweezer [i.e.,  $\tau_0$  given by Eq. (11)], for constant values of  $\sigma_\phi$  and  $h_\phi$ , there will be critical values of  $\beta$  and  $\tau_f$  in Eq. (11) corresponding to thresholds between the non-tweezed and the tweezed fundamental states. We now proceed to provide a characterization of the regions of existence of these two states for the full LL Eq. (6) and compare to the results of the NCVA with respect to the parameters  $\beta$  and  $\tau_f$ . In what follows, we study different tweezing possibilities over the parameter space spanned by  $\tau_f$ , the final temporal displacement, and  $\beta$ , the degree of adiabaticity for the speed of the tweezer. A successfully tweezed CS will correspond to a CS that stays inside the effective potential as the tweezer is displaced, while a failed attempt will result in the CS being “left behind” the dynamically evolving phase modulation profile (and, in particular, its effective confinement region).

Rather than analyzing the individual evolution of temporal profiles, we can express the various states by the power contained inside and outside of the effective confinement region of the phase modulation profile. For the full LL model, the CS temporal density  $\rho = |u|^2$  and the homogeneous state density  $\rho_0 = |v_s|^2$  can express the power inside the tweezer  $P_I(z)$  and outside the tweezer  $P_O(z)$ , which are given respectively by

$$P_I(z) = \int_{\mathcal{D}} (\rho - \rho_0) d\tau, \quad (25a)$$

$$P_O(z) = \int_{\bar{\mathcal{D}}} (\rho - \rho_0) d\tau, \quad (25b)$$

where  $\mathcal{D}$  is the domain of the tweezer which is defined as a symmetric interval around  $\tau_0$  extending to twice the tweezer width and  $\bar{\mathcal{D}}$  is the complement of  $\mathcal{D}$ . Note that we subtracted the background pedestal  $\rho_0 = |v_s|^2$ , in order to remove the effects of the pedestal (constant steady state background) and ensure the power for a CS is positive. We thus define the total power of the solution by

$$P_{\text{Tot}} = \int_{-\infty}^{+\infty} (\rho - \rho_0) d\tau = P_I + P_O.$$

For the NCVA, we use the variational parameters and construct the CS temporal density  $\bar{\rho} = |\bar{u}|^2$  and extract the power inside the tweezer  $\bar{P}_I(z)$  and outside the tweezer  $\bar{P}_O(z)$  which are given, respectively, by

$$\bar{P}_I(z) = \int_{\mathcal{D}} \bar{\rho} d\tau,$$

$$\bar{P}_O(z) = \int_{\bar{\mathcal{D}}} \bar{\rho} d\tau,$$

where  $\mathcal{D}$  and  $\bar{\mathcal{D}}$  are the same intervals described above and recall that in the construction of the NCVA ansatz we already subtracted out the effects of the background pedestal. The relative power change during the tweezing, namely between  $z = 0$  and  $z = z_f$ , is then defined by

$$Q_I = \frac{P_I(0) - P_I(z_f)}{P_{\text{Tot}}}, \quad (26a)$$

$$Q_O = \frac{P_O(0) - P_O(z_f)}{P_{\text{Tot}}}, \quad (26b)$$

for, respectively, the inside and outside of the tweezer. The same definition is used for the relative power changes ensuing from the NCVA approach.

By considering  $Q_I$  and  $Q_O$ , we can effectively find the thresholds between the various states in the relevant  $(\beta, \tau_f)$  parameter space. For example, if we begin with a steady state CS inside the tweezer at  $\tau_0 = 0$  and move with a given  $\beta$  and  $\tau_f$ , then a successfully tweezed CS will result on approximately the same powers at  $z = 0$  as  $z = z_f$  such that  $P_I(0) \approx P_I(z_f)$  as well as  $P_O(0) \approx P_O(z_f)$ , and thus resulting in power ratios  $Q_I \approx 0 \approx Q_O$ . On the contrary, if at the end of the tweezing, a bulk CS state is left in the wake of the tweezer, the resulting power changes will yield  $Q_I \approx 1$  and  $Q_O \approx -1$ .

For our analysis, as mentioned in the previous subsection, stability considerations limit us to choosing shallow tweezing potentials, namely effective potentials with small to moderate heights characterized by  $h_\phi$ . For this work, we fix  $h_\phi = 2$ . In future efforts, we will provide a more systematic analysis of the stability considerations for different phase modulation profile parameters and explore the possibilities of static and dynamic tweezing accordingly. Here, we restrict our considerations to a proof-of-principle example of a phase modulation enabling a stable static confined CS and examine the dynamical outcome for different parameters of the selected protocol  $\tau_0(z)$ . Moreover, we reiterate that all examples we discuss are limited to fixing  $u_{\text{in}} = 2$  and  $\Delta = 3.5$ .

We now report on the results having fixed the tweezer width to  $\sigma_\phi = 2$ , as mentioned earlier. The parameter space for  $\beta$  and  $\tau_f$  is discretized into 41 points between 0.1 and 20 in both directions, giving 1681 combinations for  $\tau_0(z)$  as per Eq. (11). The full LL Eq. (6) is solved using a standard second order finite difference scheme in space and a standard fourth order Runge-Kutta method in time. It is relevant to note that the integration of the NCVA system of ODEs required the use of a stiff ODE solver and thus we used Matlab's `ode15s`. Both the full LL PDE and the NCVA ODEs are evolved until  $z_f = 4z^*$ , with  $z^* = 2.5$  (see Fig. 1) which ensures that the successfully tweezed or non-tweezed CS had enough time to converge towards their respective steady states.

We will now focus on following the power ratios  $Q_I$  and  $Q_O$  from Eqs. (26) for the different parameter combinations. In order to identify the different dynamical regions, both  $Q_I$  and  $Q_O$  need to be analyzed simultaneously. Therefore, for a more compact interpretation of the results, we use the difference in power ratios, referred to

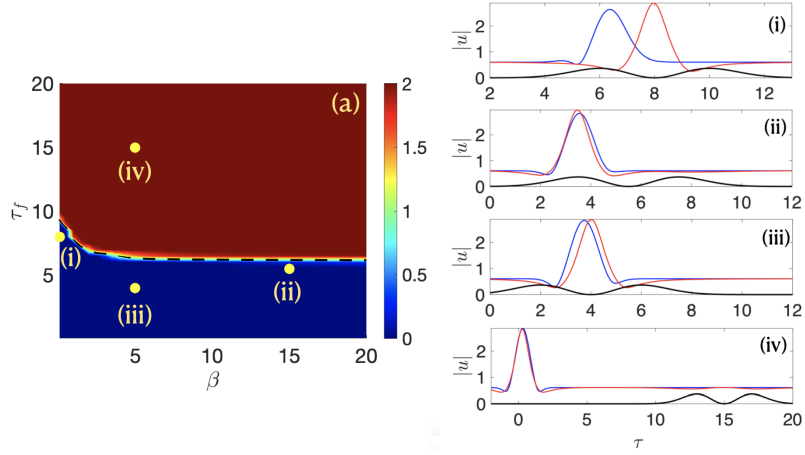


**Fig. 8** (a) The temporal tweezing map (surface plot for the tweeability index  $\Delta Q$ ), generated from the LL PDE calculations for  $z^* = 2.5$ . On this map we overlay the contour  $\Delta Q = 1$  (see black dashed line) extracted from the analogous map generated from the NCVA computations, demonstrating excellent agreement. The right panels correspond to four representative cases depicting the amplitude profiles of the NCVA (blue solid line) and LL PDE (red solid line) at  $z = 10$  alongside the effective potential profile (black solid line). The values  $(\beta, \tau_f)$  values for each case are depicted by the yellow points. The four representative cases are as follows. Panels (i) and (ii) depict two marginally tweezed CS for  $(\beta, \tau_f) = (0.1, 8)$  and  $(\beta, \tau_f) = (15, 5.5)$  (see text for details). Panel (iii) corresponds the case  $(\beta, \tau_f) = (5, 4)$  well within the tweeability region. Panel (iv) corresponds to  $(\beta, \tau_f) = (5, 15)$  well within the (red) non-tweezed region.

as the tweeability index  $\Delta Q = Q_I - Q_O$ , such that its values represent the following dynamical tweezing scenarios:

- (i)  $\Delta Q \approx 0$ : successful tweezing,
- (ii)  $\Delta Q \approx 2$ : failed tweezing, whereby the CS was left behind by the tweezer.

Figure 8(a) depicts  $\Delta Q$  as obtained from the LL PDE calculations as a function of  $\beta$  and  $\tau_f$  where the above two different tweezing regions are clearly defined: (i) successful tweezing ( $\Delta Q \approx 0$ ) in blue and (ii) failed tweezing of the CS ( $\Delta Q \approx 2$ ) in red. We note the sharp transition between these two fundamental states that could result from the dynamical tweezing. In addition to the tweezing map for the LL CS, panel (a) also depicts the overlaid contour  $\Delta Q = 1$  from the NCVA reduction (see dashed black line). We note the excellent agreement [up to the chosen discretization in the  $(\beta, \tau_f)$  plane] between the full LL tweezing map and the prediction of the reduced NCVA approach. Interestingly the boundary transition between tweezed and non-tweezed states appears to rapidly asymptote to  $\tau_f \approx 5.5$  as the degree of adiabaticity  $\beta$  is increased. The behavior of  $\Delta Q$  depicted in for Fig. 8(a) confirms the existence of two fundamental scenarios (at both LL and NCVA levels): a tweezed CS for all  $\beta$  when  $\tau_f \lesssim 5.5$  (blue region) and a non-tweezed CS (red regions). The right subpanels in Fig. 8 depict four different representative cases after the temporal tweezing attempt where the blue and red lines represent, respectively, the LL and NCVA CS while the effective potential is depicted in black. Panel (i) corresponds to the point in the left corner of the tweezed region  $(\beta, \tau_f) = (0.1, 8)$  in the tweezing map. In this extreme example, although the

the CS is successfully tweezed (i.e. confined within the region defined by the effective potential), the steering efficiency, i.e. alignment between  $\tau_0(z)$  and  $\xi(z)$  is not as effective. The success of the tweezing in turn is at the level of the integrated quantity  $\Delta Q$ , while we note the lack of perfect agreement in terms of soliton positions as predicted by the variational formulation and the LL PDE computation. Furthermore, we observe a maximal quantitative differences between the soliton centers as predicted by the NCVA and LL in this case. Panel (ii) corresponds to a CS that is tweezed with a large degree of adiabaticity  $\beta = 15$  and for  $\tau_f = 5.5$ . The amplitude of the waveforms for the LL and the NCVA CS at  $z = 10$  demonstrate very good agreement in the profiles and their corresponding soliton centers [ $\xi(z = 10) \approx 3.7$ ]. For this transitional case, we note that upon evolution to a longer fast time ( $z$ ), the LL and NCVA CS eventually catch up to the effective potential center. Panel (iii) corresponds to tweezing parameters  $(\beta, \tau_f) = (5, 4)$  well within the (blue) tweezability region. In this case, there is reasonable agreement between the respective LL and NCVA profiles. Panel (iv) corresponds to the choice  $(\beta, \tau_f) = (5, 15)$  well inside the (red) non-tweezed. Here both LL and NCVA CS waveforms at  $z = 10$  are left behind in the wake of the tweezer, with, again, very good mutual agreement in the soliton position  $\xi(z)$ .

The results presented above evidence that, with the current parameter values that we used, a combination of  $0 < \beta < 20$  with  $\tau_f \lesssim 4$  ensures a proper, successful, and efficient [in terms of alignment of  $\xi(z)$  and  $\tau_0(z)$ ] tweezing of the CS. Furthermore, we note that the NCVA provides an excellent representation of the full PDE dynamics. This is particularly of interest, as the NCVA calculations (ODE system) are far less costly than the full PDE computations, corresponding to a low (six-) dimensional representation thereof.

### 4.3 Demonstration of a Non-trivial Temporal Tweezing

Now that we have studied the parameter regions that give rise to the different tweezing scenarios, let us demonstrate the robustness of the CS manipulation when using temporal tweezer parameters  $\tau_f$  and  $\beta$  inside the tweezability region. In particular, Fig. 9 depicts a more general tweezing scenario where, instead of a single value for the parameters  $\tau_f$  and  $\beta$ , we change the parameters at set increments in  $z$ . Specifically, we choose a nontrivial back-and-forth tweezing “trajectory” with a zigzagging motion separated in six subintervals with different degrees of adiabaticity as follows. For  $0 \leq z < 5$ ,  $\tau_f(0) = 0$ , and  $\beta = 1$ , then for  $5 \leq z < 10$ ,  $\tau_f(5) = 2$ , and  $\beta = 2$ , then for  $10 \leq z < 15$ ,  $\tau_f(10) = 1$ , and  $\beta = 3$ , then for  $15 \leq z < 20$ ,  $\tau_f(15) = 2$ , and  $\beta = 2$ , then for  $20 \leq z < 25$ ,  $\tau_f(20) = 1$ , and  $\beta = 0.5$ , then for  $25 \leq z < 30$ ,  $\tau_f(25) = -1$ , and  $\beta = 3$ . As Fig. 9 shows, the CS is successfully tweezed along this complicated zigzagging orbit (see middle white dashed curve), thus showcasing the robustness of the tweezing mechanism for the full LL dynamics [shown in panel (a)]. Furthermore, as panel (b) shows, the NCVA reduction of the LL system is also able to predict and reproduce the successful tweezing of the CS along the zigzagging orbit with a very good quantitative agreement with the full PDE LL calculations. This is also reflected in panel (c) where the soliton center  $\xi$  is extracted from the LL PDE calculations (black dashed line) together with the variational parameter  $\xi(z)$  demonstrating good quantitative agreement as well. Finally, in panel (d) we depict the LL (red solid line)

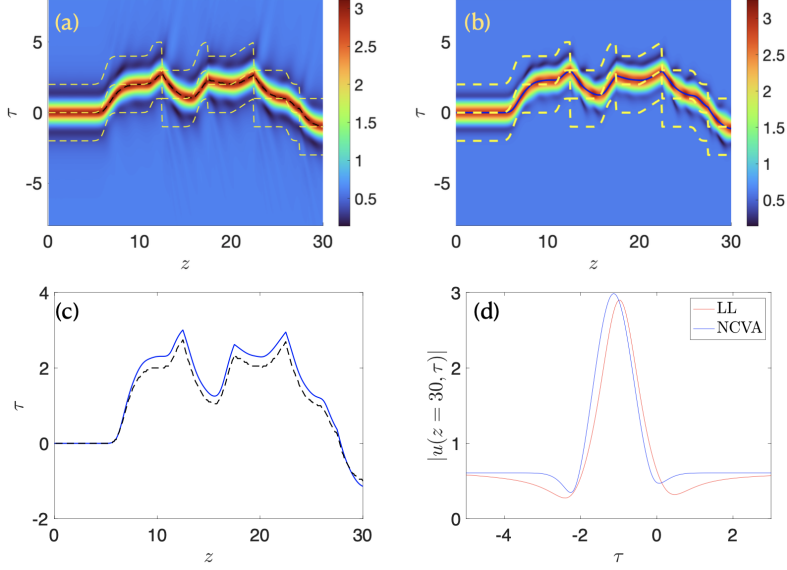


**Fig. 9** Dynamic evolution of a CS using a zigzagging tweezer with different degrees of adiabaticity by varying  $\tau_f$  and  $\beta$  (see text for details). These computations were performed by fixing  $z^* = 1.25$  [see Eq. (11)]. (a) The surface plot of the wave amplitude  $|u|$  from the LL model. We overlay the soliton center  $\xi(z)$  (black dashed line) and tweezer center  $\tau_0(z)$  (central yellow dashed line). We also show the maxima of the effective potential  $\tau_0(z) \pm \sigma_\phi$  in yellow dashed lines, depicting the extents of the soliton waveguide. (b) Same as (a), but generated from the NCVA ODE calculations. Here the NCVA soliton center of mass  $\xi(z)$  is shown in blue solid line. (c) CS tweezed trajectories for the LL model (black dashed) and NCVA reduction (blue solid) that continue to follow the prescribed trajectory despite the tweezer being moved back-and-forth at various speeds. (d) CS wave profiles of the LL (red solid) and NCVA (blue solid) at final time  $z = 30$ , which also demonstrate reasonable quantitative agreement. This example serves to illustrate how a CS can be robustly manipulated given various degrees of adiabaticity.

and NCVA (blue solid line) CSs at the end of this complex tweezing scenario, demonstrating again a good agreement between the original LL PDE model and its NCVA ODE reduction. This tweezing example suggests that, through an appropriate manipulation of the phase-modulation of the holding beam, it is possible to trap and move the CS at will, based on the proposed tweezing mechanism and for a (revealed herein) wide interval of the associated dynamical parameters. Furthermore, examining the dynamics on a soliton manifold (NCVA calculations) yields valuable insights into the full dynamics, while enabling a computational platform that is significantly cheaper.

## 5 Conclusions and Future Challenges

In Ref. [4] the authors showed experimentally that a cavity soliton (CS) stored in a passive loop of an optical fiber could be temporally tweezed by manipulating the phase-modulation of the holding beam. Motivated by this experimental work, we studied herein the possibility of tweezing more generally CSs using various profiles of the holding beam and in particular varying the degree of adiabaticity used in the tweezing

“trajectory”. We modeled the system using a variant of the complex Ginzburg-Landau (cGL) equation in the form of the Lugiato-Lefever (LL) partial differential equation with additional terms accounting for the incorporation of the tweezer from the phase-modulation of the holding beam.

In our study, we assume a Gaussian phase-modulation that gives rise to an effective tweezer potential, related to the derivative of the phase-modulation profile, that takes the shape of a localized trapping profile. We find that, depending on the tweezer parameters, the following two different outcomes are possible. (a) For sufficiently slow (adiabatic) tweezing motion, the tweezer is generically capable of transporting the CS to any desired location. (b) On the other hand, for relatively large tweezer speeds the CS slides out of the tweezing potential and is left behind to exist in the bulk of the medium while the tweezer moves away without carrying along the CS. As part of our theoretical study, we develop a Lagrangian formalism for the modified the LL equation that intrinsically includes gain and loss terms. To tackle this out-of-equilibrium, non-Hamiltonian system we use the recently developed non-conservative variational approximation (NCVA) of Ref. [24], based on the earlier formulation of Refs. [42, 43]. We use the NCVA approach with an appropriately crafted CS ansatz to reduce the original LL dynamics (a partial differential equation) to a set of coupled ordinary differential equations on the ansatz parameters (height, position, width, phase, velocity, and chirp). We show how the NCVA reduction approach is able to qualitatively, and to a significant extent quantitatively, describe the different tweezing scenarios. In particular, we notice that the NCVA is capable of predicting quite accurately the threshold in the tweezer parameter space.

Our analysis of not only static, but also dynamical tweezing offers insights into the design of localized tweezers used in optical information processing, in turn enabling the potential trapping of ultrashort pulses of light and dynamical moving of those around in time, with respect to, and independently of other pulses of light. Furthermore, from our study of the LL equation and the NCVA approach, we have developed a process to identify regions of tweezability which can aid toward the experimental design and identification of regimes of reliable temporal tweezing used for information processing.

A possible extension of this work pertains the case of a periodic modulation of the holding beam that induces a periodic effective tweezer potential. It would be interesting to study in detail the possible manipulation of the CSs using such periodic (or even quasi-periodic) modulation as it was studied in Refs. [20, 21] for the (otherwise conservative) nonlinear Schrödinger case. Another avenue of potential interest would be the study of tweezability of not only cavity solitons but also vortices in two-dimensional settings in the presence of gain and loss similar to what has been reported in the conservative case of the nonlinear Schrödinger equation; see Refs. [47, 48] and references therein. In general, the extension of considerations presented herein for one spatial dimension to the context of higher-dimensional settings would be a particularly interesting direction for future work.

In reference to temporal tweezing, multiple CSs can be present simultaneously and independently at arbitrary locations in a passive loop of optical fiber. Therefore, a relevant extension would be to add interactions of multiple CSs in the system. Indeed, a systematic study of the nonlinear states in the present setting and of their properties

would be of interest in its own right. In addition, investigating the dynamics, interactions, and tweeability of the CS by allowing for long-range soliton interactions is necessary to understand an effective treatment of a CS, each of which constitute an ideal bit in optical information processing. It is relevant to mention in that regard that the recent review of Ref. [49] has summarized the extensive control that this framework enables both in the way of phase, as well as of intensity of the inhomogeneous driving field. Additionally, recent experiments of pulsed driving are also discussed therein towards the direction of producing flexible and efficient optical frequency combs. Another possible extension of the temporal tweezing study is to analyze the linearization spectrum of the system and identify the (in)stability transitions between the different states we identified. This type of analysis can be extended from statically tweezed states to potential traveling ones. Indeed, it would be interesting to identify the co-traveling states in the case of a traveling tweezer and to identify whether the transition, e.g., from tweezing to disappearance of the pulse can be identified with a bifurcation phenomenon. Such directions are currently in progress and will be reported in future publications.

## Appendix A NCVA System of Equations for Temporal Tweezing of Cavity Soliton

In this Appendix, we present the resulting modified Euler-Lagrange equations of motion from the LL Eq. (6) for temporal tweezing based on the NCVA where the over-dot denotes derivative with respect to  $z$ . Before presenting these equations, we provide the effective Lagrangian  $\bar{L}$  evaluated on the Gaussian ansatz Eq. (18):

$$\begin{aligned} \bar{L} = & \sqrt{\pi}(-c\xi + b)a^2\sigma + \frac{\sqrt{\pi}a^2\sigma^3}{2}d + \frac{\sqrt{\pi}a^2}{2\sigma} + 2\sqrt{\pi}a^2d^2\sigma^3 + \sqrt{\pi}a^2c^2\sigma - \frac{\sqrt{2\pi}a^4\sigma}{4} \\ & + \Delta\sqrt{\pi}a^2\sigma + \frac{\sqrt{\pi}e}{(\sigma^2 + \sigma_\phi^2)^{5/2}} \frac{-\frac{\tau_0^2 - 2\tau_0\xi + \xi^2}{\sigma_\phi^2 + \sigma^2} h_\phi^2 \sigma_\phi \sigma (\tau_0 - \xi)^2 a^2}{(\sigma^2 + \sigma_\phi^2)^{5/2}} + \frac{\sqrt{\pi}e}{2\sigma_\phi(\sigma_\phi^2 + \sigma^2)^{3/2}} \frac{-\frac{\tau_0^2 - 2\tau_0\xi + \xi^2}{\sigma_\phi^2 + \sigma^2} h_\phi^2 a^2 \sigma^3}{(\sigma^2 + \sigma_\phi^2)^{3/2}} \\ & - 2\sqrt{\pi}|v_s|^2 a^2 \sigma + \frac{4\sqrt{2\pi}e}{(2\sigma_\phi^2 + \sigma^2)^{5/2}} \frac{-\frac{\tau_0^2 - 2\tau_0\xi + \xi^2}{2\sigma_\phi^2 + \sigma^2} h_\phi \sigma_\phi \sigma (\tau_0 - \xi) a^2 (2d\sigma^2\tau_0 - 2d\sigma^2\xi + 2\sigma_\phi^2 c + c\sigma^2)}{(2\sigma_\phi^2 + \sigma^2)^{5/2}} \\ & - \frac{4\sqrt{2\pi}e}{(2\sigma_\phi^2 + \sigma^2)^{3/2}} \frac{-\frac{\tau_0^2 - 2\tau_0\xi + \xi^2}{2\sigma_\phi^2 + \sigma^2} h_\phi \sigma_\phi \sigma^3 a^2 d}{(2\sigma_\phi^2 + \sigma^2)^{3/2}}. \end{aligned} \quad (\text{A1})$$

Substituting the expression for the effective Lagrangian into the modified Euler-Lagrange equations Eqs. (13) yields the following explicit ODE system (obtained using Maple):

$$\begin{aligned} \dot{a} = & \frac{-2}{\sqrt{\pi}a\sigma^3(2\sigma_\phi^2 + \sigma^2)^{5/2}} \left[ -\sqrt{2\pi}\sigma_\phi h_\phi \sigma^3 a^2 e^{-\frac{(\xi - \tau_0)^2}{2\sigma_\phi^2 + \sigma^2}} (\sigma^2 - 2(\xi - \tau_0 + \sigma_\phi)(\xi - \tau_0 - \sigma_\phi)) \right. \\ & \left. + (2\sigma_\phi^2 + \sigma^2)^{5/2} \left( \sqrt{\pi}a^2 d \sigma^3 - \frac{3\sigma^2}{8} I_b + \frac{I_d}{4} \right) \right] \end{aligned} \quad (\text{A2})$$

$$\begin{aligned} \dot{b} = & -\frac{3}{4\sqrt{\pi}a^2\sigma^2\sigma_\phi(2\sigma_\phi^2+\sigma^2)^{9/2}(\sigma_\phi^2+\sigma^2)^{9/2}} \times \\ & \left[ -\frac{5\sigma_\phi(2\sigma_\phi^2+\sigma^2)^{9/2}(\sigma_\phi^2+\sigma^2)^{9/2}}{6} \left( a^2\sqrt{\pi} \left( -\frac{8}{5} + \sqrt{2}a^2\sigma^2 + \frac{8}{5}(c^2+2|v_s|^2-\Delta)\sigma^2 \right) - \frac{6\sigma}{5}(aI_a - \frac{4cI_c}{3} \right. \right. \\ & \left. \left. - \frac{2\sigma I_s}{3} \right) - 8\sqrt{2\pi}h_\phi\sigma_\phi^2a^2\sigma^4(\sigma_\phi^2+\sigma^2)^{9/2}e^{-\frac{(\xi-\tau_0)^2}{\sigma_\phi^2+\sigma^2}} \left( \delta_1\sigma^6 + \delta_2\sigma^4 + \delta_3\sigma^2 + \delta_4 \right) \right. \\ & \left. \left. + \sqrt{\pi}h_\phi^2a^2\sigma^2(2\sigma_\phi^2+\sigma^2)^{9/2}e^{-\frac{(\xi-\tau_0)^2}{\sigma_\phi^2+\sigma^2}} \left( \sigma^8 + \delta_5\sigma^6 + \delta_6\sigma^4 + \delta_7\sigma^2 + \delta_8 \right) \right] \right] \end{aligned} \quad (\text{A3})$$

$$\begin{aligned} \dot{c} = & \frac{-24}{\sqrt{\pi}a^2\sigma\sigma_\phi(\sigma_\phi^2+\sigma^2)^{7/2}(2\sigma_\phi^2+\sigma^2)^{7/2}} \left[ \sqrt{2\pi}(\sigma_\phi^2+\sigma^2)^{7/2}\sigma_\phi^2\sigma h_\phi a^2e^{-\frac{(\xi-\tau_0)^2}{2\sigma_\phi^2+\sigma^2}} \times \right. \\ & \left( \left( d\xi - d\tau_0 - \frac{c}{6} \right) \sigma^4 + \left( -\frac{2d\xi^3}{3} + (2d\tau_0 + \frac{c}{3})\xi^2 + 2(-\frac{c\tau_0}{3} + (\sigma_\phi^2 - \tau_0^2)d)\xi + \frac{(\tau_0^2 - 2\sigma_\phi^2)c}{3} + 2d\tau_0(\tau_0^2 - 3\sigma_\phi^2) \right) \sigma^2 \right. \\ & \left. + \frac{2\sigma_\phi^2c(\xi - \tau_0 + \sigma_\phi)(\xi - \tau_0 - \sigma_\phi)}{3} \right) - \frac{(2\sigma_\phi^2+\sigma^2)^{7/2}}{24} \left( -(\sigma_\phi^2+\sigma^2)^{7/2}\sigma_\phi(I_b c + I_\xi) \right. \\ & \left. \left. + (\xi - \tau_0)\sigma\sqrt{\pi}h_\phi^2a^2e^{-\frac{(\xi-\tau_0)^2}{\sigma_\phi^2+\sigma^2}} \left( \sigma^4 - \sigma_\phi^2\sigma^2 + 2\sigma_\phi^2(\xi - \tau_0 + \sigma_\phi)(\xi - \tau_0 - \sigma_\phi) \right) \right) \right] \end{aligned} \quad (\text{A4})$$

$$d = -\frac{1}{4\sqrt{\pi}a^2\sigma^4} \left( a^2\sqrt{\pi}(16d^2\sigma^4 + \sqrt{2}a^2\sigma^2 - 4) - 2aI_a\sigma + 4I_\sigma\sigma^2 \right) \quad (\text{A5})$$

$$\begin{aligned} & -\frac{4}{\sqrt{\pi}a^2\sigma^4\sigma_\phi(\sigma_\phi^2+\sigma^2)^{9/2}(2\sigma_\phi^2+\sigma^2)^{9/2}} \left[ \sqrt{2\pi}(\sigma_\phi^2+\sigma^2)^{9/2}\sigma_\phi^2\sigma^4h_\phi a^2e^{-\frac{(\xi-\tau_0)^2}{2\sigma_\phi^2+\sigma^2}} \times \right. \\ & \left( d\sigma^6 + \delta_9\sigma^4 + \delta_{10}\sigma^2 + \delta_{11} \right) - \frac{(2\sigma_\phi^2+\sigma^2)^{9/2}}{8} a^2\sqrt{\pi}h_\phi^2e^{-\frac{(\xi-\tau_0)^2}{\sigma_\phi^2+\sigma^2}} \sigma^4 \left( \sigma^6 + \delta_{12}\sigma^4 + \delta_{13}\sigma^2 + \delta_{14} \right) \left. \right] \end{aligned} \quad (\text{A6})$$

$$\begin{aligned} \dot{\sigma} = & \frac{4}{\sqrt{\pi}a^2\sigma^2(2\sigma_\phi^2+\sigma^2)^{5/2}} \left[ -\sqrt{2\pi}\sigma_\phi h_\phi\sigma^3a^2e^{-\frac{(\xi-\tau_0)^2}{2\sigma_\phi^2+\sigma^2}} \left( \sigma^2 - 2(\xi - \tau_0 + \sigma_\phi)(\xi - \tau_0 - \sigma_\phi) \right) \right. \\ & \left. + (2\sigma_\phi^2+\sigma^2)^{5/2} \left( \sqrt{\pi}a^2d\sigma^3 - \frac{\sigma^2 I_b}{8} + \frac{I_d}{4} \right) \right] \end{aligned} \quad (\text{A7})$$

$$\begin{aligned} \dot{\xi} = & \frac{-4}{\sqrt{\pi}(2\sigma_\phi^2+\sigma^2)^{3/2}a^2\sigma} \left[ \sqrt{2\pi}\sigma_\phi h_\phi a^2\sigma(\xi - \tau_0)e^{-\frac{(\xi-\tau_0)^2}{2\sigma_\phi^2+\sigma^2}} \right. \\ & \left. - \sqrt{2\sigma_\phi^2+\sigma^2} \left( \sqrt{\pi}c\sigma a^2 + \frac{I_c}{2} \right) \left( \sigma_\phi^2 + \frac{\sigma^2}{2} \right) \right] \end{aligned} \quad (\text{A8})$$

where

$$\begin{aligned} \delta_1 &= d, \\ \delta_2 &= -4d\xi^2 + (8d\tau_0 + c)\xi - c\tau_0 + 4d(\sigma_\phi^2 - \tau_0^2), \\ \delta_3 &= 2 \left[ \frac{2d}{3}\xi^4 + \frac{(-8d\tau_0 - c)}{3}\xi^3 + (c\tau_0 + 4d(\tau_0^2 - \sigma_\phi^2))\xi^2 \right. \end{aligned}$$

$$\begin{aligned}
& + \left( (2\sigma_\phi^2 - \tau_0^2) c - \frac{8d\tau_0}{3} (\tau_0^2 - 3\sigma_\phi^2) \right) \xi \\
& + \left( -2\tau_0\sigma_\phi^2 + \frac{1}{3}\tau_0^3 \right) c + \frac{2d}{3} (3\sigma_\phi^4 - 6\tau_0^2\sigma_\phi^2 + \tau_0^4) \Big], \\
\delta_4 &= -\frac{4c\sigma_\phi^2}{3}(\xi - \tau_0) \left( (\xi - \tau_0)^2 - 3\sigma_\phi^2 \right), \\
\delta_5 &= 2 \left( -\frac{\xi^2}{3} - \frac{\tau_0^2}{3} + \sigma_\phi^2 + \frac{2\tau_0\xi}{3} \right), \\
\delta_6 &= 4\sigma_\phi^2 \left( \xi^2 - 2\tau_0\xi + \tau_0^2 + \frac{\sigma_\phi^2}{4} \right), \\
\delta_7 &= -\frac{4\sigma_\phi^2}{3}(\xi - \tau_0)^2 \left( (\xi - \tau_0)^2 - \frac{9\sigma_\phi^2}{2} \right), \\
\delta_8 &= \frac{4\sigma_\phi^6}{3}(\xi - \tau_0)^2, \\
\delta_9 &= -8(\xi - \tau_0)(d\xi - d\tau_0 - \frac{3c}{8}), \\
\delta_{10} &= 2 \left( 2d\xi^4 + (-8d\tau_0 - c)\xi^3 + (-4d(\sigma_\phi^2 - 3\tau_0^2) + 3c\tau_0) \xi^2 \right. \\
& + (8\tau_0d(\sigma_\phi^2 - \tau_0^2) - 3c(\tau_0^2 - 2\sigma_\phi^2)) \xi \\
& + 2d(-3\sigma_\phi^4 - 2\tau_0^2\sigma_\phi^2 + \tau_0^4) + \tau_0c(\tau_0^2 - 6\sigma_\phi^2) \Big), \\
\delta_{11} &= 16\sigma_\phi^2 \left[ -\frac{c}{4}\xi^3 + \left( d\sigma_\phi^2 + \frac{3c\tau_0}{4} \right) \xi^2 + \left( -2d\tau_0\sigma_\phi^2 + \frac{3c}{4}(\sigma_\phi^2 - \tau_0^2) \right) \xi \right. \\
& + \left. \sigma_\phi^2(\tau_0^2 - \sigma_\phi^2)d + \frac{\tau_0c}{4}(\tau_0^2 - 3\sigma_\phi^2) \right], \\
\delta_{12} &= -2(\xi - \tau_0)^2, \\
\delta_{13} &= 8\sigma_\phi^2 \left( (\xi - \tau_0)^2 - \frac{3}{8}\sigma_\phi^2 \right), \\
\delta_{14} &= -4\sigma_\phi^2 \left( \xi^4 - 4\tau_0\xi^3 + \left( 6\tau_0^2 - \frac{5\sigma_\phi^2}{2} \right) \xi^2 + (5\tau_0\sigma_\phi^2 - 4\tau_0^3) \xi \right. \\
& + \left. \tau_0^4 - \frac{5\sigma_\phi^2}{2}\tau_0^2 + \frac{\sigma_\phi^4}{2} \right). \tag{A9}
\end{aligned}$$

## Declarations

- **Ethics approval and consent to participate:** Not applicable
- **Consent for publication:** Not applicable

- **Availability of data and materials:** Not applicable
- **Competing interests:** The authors have no relevant financial or non-financial interests to disclose. The authors have no competing interests to declare that are relevant to the content of this article.
- **Funding:** RCG acknowledges the support from NSF-1603058 and NSF-2110038. PGK acknowledges the support from NSF-2204702 and NSF-2110030.
- **Authors' contributions:** All authors contributed equally.
- **Acknowledgements:** Not applicable

## References

- [1] Ashkin, A.: Acceleration and trapping of particles by radiation pressure. *Phys. Rev. Lett.* **24**, 156 (1970)
- [2] Ashkin, A., Dziedzic, J.M., Bjorkholm, J.E., Chu, S.: Observation of a single-beam gradient force optical trap for dielectric particles. *Opt. Lett.* **11**, 288 (1986)
- [3] Chu, S., Bjorkholm, J.E., Ashkin, A., Cable, A.: Experimental observation of optically trapped atoms. *Phys. Rev. Lett.* **57**, 314 (1986)
- [4] Jang, J.K., Erkintalo, M., Coen, S., Murdoch, S.G.: Temporal tweezing of light through the trapping and manipulation of temporal cavity solitons. *Nat. Commun.* **6**, 7370 (2015)
- [5] Firth, W.J., Weiss, C.O.: Cavity and feedback solitons. *Opt. Photonics News* **13**, 54–58 (2002)
- [6] Lugiato, L.A.: Introduction to the feature section on cavity solitons: an overview. *IEEE J. Quantum Elec.* **39**, 193–196 (2003)
- [7] Boyd, R.W., Gauthier, D.J., Gaeta, A.L.: Applications of slow light in telecommunications. *Opt. Photonics News* **17**, 18–23 (2006)
- [8] Hau, L.V.: Optical information processes in Bose-Einstein condensates. *Nat. Photon.* **2**, 451–453 (2008)
- [9] Hau, L.V., Harris, S.E., Dutton, Z., Behroozi, C.H.: Light speed reduction to 17 metres per second in an ultracold atomic gas. *Nature* **397**, 594–598 (1999)
- [10] Okawachi, Y., Bigelow, M.S., Sharping, J.E., Zhu, Z., Schweinsberg, A., Gauthier, D.J., Boyd, R.W., Gaeta, A.L.: Tunable all-optical delays via Brillouin slow light in an optical fiber. *Phys. Rev. Lett.* **94**, 153902 (2005)
- [11] Mok, J.T., Sterke, C.M., Littler, I.C.M., Eggleton, B.J.: Dispersionless slow light using gap solitons. *Nature Phys.* **2**, 775–780 (2006)
- [12] Thévenaz, L.: Slow and fast light in optical fibers. *Nat. Photon.* **2**, 474–481 (2008)

- [13] Rothenberg, J.E.: Intrafiber visible pulse compression by cross-phase modulation in a birefringent optical fiber. *Opt. Lett.* **15**, 495 (1990)
- [14] Sterke, C.M.: Optical push broom. *Opt. Lett.* **17**, 914 (1992)
- [15] Nishizawa, N., Goto, T.: Ultrafast all optical switching by use of pulse trapping across zero-dispersion wavelength. *Opt. Express* **11**, 359 (2003)
- [16] Gorbach, A.V., Skryabin, D.V.: Light trapping in gravity-like potentials and expansion of supercontinuum spectra in photonic-crystal fibres. *Nat. Photon.* **1**, 653 (2007)
- [17] Philbin, T.G., Kuklewicz, C., Robertson, S., Hill, S., König, F., Leonhardt, U.: Fiber-optical analog of the event horizon. *Science* **319**, 1367 (2008)
- [18] Webb, K.E., Erkintalo, M., Xu, Y., Broderick, N.G.R., Dudley, J.M., Genty, G., Murdoch, S.G.: Nonlinear optics of fibre event horizons. *Nat. Commun.* **5**, 4969 (2014)
- [19] Nistazakis, H.E., Kevrekidis, P.G., Malomed, B.A., Frantzeskakis, D.J., Bishop, A.R.: Targeted transfer of solitons in continua and lattices. *Phys. Rev. E* **66**, 015601 (2002)
- [20] Kevrekidis, P.G., Frantzeskakis, D.J., Carretero-González, R., Malomed, B.A., Herring, G., Bishop, A.R.: Statics, dynamics and manipulation of bright matter-wave solitons in optical lattices. *Phys. Rev. A* **71**, 023614 (2005)
- [21] Porter, M.A., Kevrekidis, P.G., Carretero-González, R., Frantzeskakis, D.J.: Dynamics and manipulation of matter-wave solitons in optical superlattices. *Phys. Lett. A* **352**, 210 (2006)
- [22] He, Y.J., Malomed, B.A., Wang, H.Z.: Steering the motion of rotary solitons in radial lattices. *Phys. Rev. A* **76**, 053601 (2007)
- [23] English, L.Q., Palmero, F., Sievers, A.J., Kevrekidis, P.G., Barnak, D.H.: Traveling and stationary intrinsic localized modes and their spatial control in electrical lattices. *Phys. Rev. E* **81**, 046605 (2010)
- [24] Rossi, J., Carretero-González, R., Kevrekidis, P.G.: Non-conservative variational approximation for nonlinear Schrödinger equations. *Eur. Phys. J. Plus* **135**, 854 (2020)
- [25] Aranson, I.S., Kramer, L.: The world of the complex Ginzburg-Landau equation. *Rev. Mod. Phys.* **74**, 99–143 (2002)
- [26] García-Morales, V., Krischer, K.: The complex Ginzburg-Landau equation: an introduction. *Contemporary Physics* **53**(2), 79–95 (2012)

- [27] Leo, F., Coen, S., Kockaert, P., Gorza, S.-P., Emplit, P., Haelterman, M.: Temporal cavity solitons in one-dimensional Kerr media as bits in an all-optical buffer. *Nat. Photon.* **4**, 471–476 (2010)
- [28] Jang, J.K., Erkintalo, M., Murdoch, S.G., Coen, S.: Ultraweak long-range interactions of solitons observed over astronomical distances. *Nat. Photon.* **7**, 657 (2013)
- [29] Wabnitz, S.: Suppression of interactions in a phase-locking soliton optical memory. *Opt. Lett.* **18**, 601 (1993)
- [30] Leo, F., Gelens, L., Emplit, P., Haelterman, M., Coen, S.: Dynamics of one-dimensional Kerr cavity solitons. *Opt. Express* **21**, 9180 (2013)
- [31] Jang, J.K., Erkintalo, M., Murdoch, S.G., Coen, S.: Observation of dispersive wave emission by temporal cavity solitons. *Opt. Lett.* **39**, 5503 (2014)
- [32] Grelu, P., Akhmediev, N.: Dissipative solitons for mode-locked lasers. *Nat. Photon.* **6**, 84 (2012)
- [33] Leo, F., Coen, S., Kockaert, P., Gorza, S.-P., Emplit, P., Haelterman, M.: Temporal cavity solitons in one-dimensional Kerr media as bits in an all-optical buffer. *Nat. Photon.* **4**, 471 (2012)
- [34] Lugiato, L.A., Lefever, R.: Spatial dissipative structures in passive optical systems. *Phys. Rev. Lett.* **58**, 2209–2211 (1987)
- [35] Haelterman, M., Trillo, S., Wabnitz, S.: Dissipative modulation instability in a nonlinear dispersive ring cavity. *Opt. Commun.* **91**, 401–407 (1992)
- [36] Grelu, P. (ed.): *Nonlinear Optical Cavity Dynamics: From Microresonators to Fiber Lasers*. Wiley-VCH Verlag GmbH & Co. KGaA, Weinheim, Germany (2016)
- [37] Gomila, D., Scroggie, A.J., Firth, W.J.: Bifurcation structure of dissipative solitons. *Physica D* **227**, 70–77 (2007)
- [38] Firth, W.J., Scroggie, A.J.: Optical bullet holes: Robust controllable localized states of a nonlinear cavity. *Phys. Rev. Lett.* **76**, 1996 (1996)
- [39] Parra-Rivas, P., Gomila, D., Matías, M.A., Colet, P., Gelens, L.: Effects of inhomogeneities and drift on the dynamics of temporal solitons in fiber cavities and microresonators. *Opt. Express* **22**, 30943–30954 (2014)
- [40] Theocharis, G., Kevrekidis, P.G., Frantzeskakis, D.J., Schmelcher, P.: Symmetry breaking in symmetric and asymmetric double-well potentials. *Phys. Rev. E* **74**, 056608 (2006)

- [41] Ablowitz, M.J., Prinari, B., Trubatch, A.D.: Discrete and Continuous Nonlinear Schrödinger Systems. Cambridge University Press, Cambridge (2004)
- [42] Galley, C.R.: Classical mechanics of nonconservative systems. *Phys. Rev. Lett.* **110**, 174301 (2013)
- [43] Galley, C.R., Tsang, D., Stein, L.C.: The principle of stationary nonconservative action for classical mechanics and field theories. arXiv:1412.3082 [math-ph] (2014)
- [44] Galley, C.R., Tsang, D., Stein, L.C.: The principle of stationary nonconservative action for classical mechanics and field theories (2014)
- [45] Rossi, J., Carretero-González, R., Kevrekidis, P.G., Haragus, M.: On the spontaneous time-reversal symmetry breaking in synchronously-pumped passive Kerr resonators **49**, 455201 (2016)
- [46] Kevrekidis, P.G., Frantzeskakis, D.J., Carretero-González, R.: The Defocusing Nonlinear Schrödinger Equation: From Dark Solitons to Vortices and Vortex Rings. SIAM, Philadelphia (2015)
- [47] Davis, M.C., Carretero-González, R., Shi, Z., Law, K.J.H., Kevrekidis, P.G., Anderson, B.P.: Manipulation of vortices by localized impurities in Bose-Einstein condensates. *Phys. Rev. A* **80**, 023604 (2009)
- [48] Gertjerenken, B., Kevrekidis, P.G., Carretero-González, R., Anderson, B.P.: Generating and manipulating quantized vortices on-demand in a Bose-Einstein condensate: a numerical study. *Phys. Rev. A* **93**, 023604 (2016)
- [49] Erkintalo, M., Murdoch, S.G., Coen, S.: Phase and intensity control of dissipative Kerr cavity solitons. *Journal of the Royal Society of New Zealand* **52**(2), 149–167 (2022)
- [50] Quarteroni, A., Sacco, R., Saleri, F.: Numerical mathematics. Springer Science & Business Media (2006)
- [51] Yang, J.: Newton-conjugate-gradient methods for solitary wave computations. *Journal of Computational Physics* (2009)
- [52] Kelley, C.T.: Solving nonlinear equations with Newton’s method. SIAM (2003)